JOURNAL OF Applied Polymer SCIENCE

Multiphysics Simulations of Cure Residual Stresses and Springback in a Thermoset Resin Using a Viscoelastic Model with Cure-Temperature-Time Superposition

Bhaskar Patham
Material Characterization and Modeling Group, India Science Lab, General Motors Global Research and Development, GM Technical Centre India Pvt. Ltd., Creator Building, International Tech Park Ltd., Whitefield Road, Bangalore 560 066, India
Correspondence to: B. Patham (E-mail: bhaskar.patham@gm.com)

ABSTRACT: Simulations of evolution of cure-induced stresses in a viscoelastic thermoset resin are presented. The phenomenology involves evolution of resin modulus with degree of cure and temperature, the development of stresses due to crosslink induced shrinkage, and the viscoelastic relaxation of these stresses. For the simulations, the detailed kinetic and chemo-thermo-rheological models for an epoxy-amine thermoset resin system, described in Eom et al. (*Polym. Eng. Sci.* 2000, 40, 1281) are employed. The implementation of this model into the simulation is facilitated by multiphysics simulation strategies. The trends in simulated cure-induced stresses obtained using the full-fledged viscoelastic model are compared with those obtained from two other equivalent material models, one involving a constant elastic modulus, and the other involving a cure-dependent (but time-invariant) elastic modulus. It is observed that the viscoelastic model not only results in lower estimates of cure-induced stresses, but also provides subtle details of the springback behavior. © 2012 Wiley Periodicals, Inc. J. Appl. Polym. Sci. 000: 000–000, 2012

KEYWORDS: thermosets; theory and modeling; kinetics; rheology; viscosity and viscoelasticity

Received 8 May 2012; accepted 23 September 2012; published online
DOI: 10.1002/app.38744

INTRODUCTION

Accurate predictions of residual stresses in thermoset resins, adhesives, and composites require detailed accounting of multiple phenomena—mold-part interaction, cure shrinkage strains, thermal strains, the kinetics of resin cure, and the evolution of the resin properties with temperature and degree of cure. Residual stress development and shape distortions in thick thermoset sections are further influenced by large temperature gradients across the thickness driven by the exothermic heat of reaction. The resin modulus, a key parameter governing the magnitude of residual stresses, is a strong function of the degree of cure (α) and the temperature history. During the course of crosslinking, the resin, starting from a viscous state, can evolve into a rubbery gel (a ductile thermoset) or, upon vitrification, become a glass (a brittle thermoset). In addition to cure and temperature dependence, the curing resin also displays time dependent stress relaxation, governed by intrinsic relaxation times that are functions of the degree of cure and the temperature.[1–4]

To describe accurately the evolution of stresses within a thermoset during cure, it is imperative to capture in detail the time-, cure, and temperature dependent evolution of the resin modulus. Complex kinetic and thermo-chemo-rheological models that account for diffusion effects in kinetics and rheological complexity of the curing resin have traditionally been difficult to implement in finite element schemes, necessitating simplifying assumptions. With the development of advanced computational methods involving multiphysics capabilities this complexity may be addressed in a logical fashion. In this report, multiphysics based finite element simulations of evolution of cure-induced residual stresses in a thermoset system are presented. The simulations employ a comprehensive semiempirical material model developed by Eom et al.[1] The kinetic and chemo-thermo-rheological model described by Eom et al, captures in detail the cure- and temperature-dependence of the viscoelastic stresses within the curing resin while accounting for the chemo-thermo-rheological complexity of the curing resin (different mechanisms of stress relaxation prior to and post gelation). Diffusion limited regimes in the cure kinetics of the thermoset are also accounted for in this scheme.

BACKGROUND: CHEMO-THERMO-RHEOLOGICAL MODELS FOR CURING THERMOSETS

The instantaneous stress $\sigma(t)$ in a curing thermoset resin during relaxation following the application of a strain γ is represented

in the form of a relaxation modulus, $G_r(t) = \sigma(t)/\gamma$. The relaxation modulus is a very strong function of the temperature of curing and the degree of cure (with additional relaxation mechanisms introduced at gel point ($\alpha = \alpha_{gel}$) where the relaxation curve starts developing a prominent rubbery plateau). A comprehensive time-temperature-cure superposition model, that correlates in detail the stress relaxation behavior $G_r(t, T, \alpha)$ at any given temperature, T, and degree of cure, α, to that at a given reference temperature (T_{ref}) and the reference conversion (α_{ref}) needs to be arrived at.[1–4] This generic framework, using a generalized multimode Maxwell model, with each relaxation mode i characterized by a stiffness, G_i, and a relaxation time constant, λ_i (Ref. 4), may be described as below

$$G_r(t, T, \alpha) = G_\infty + \sum_{i=1}^{p} G_i(\alpha_{ref}) A_G \exp\left[\frac{-t}{(\lambda_{i,T_{ref}\alpha_{ref}} A_T A_\alpha)}\right] \quad (1)$$

$$G_0(T, \alpha) = G_\infty + \sum_{i=1}^{p} G_i(\alpha_{ref}) A_G$$

$$A_T|_{\alpha_{ref}} = \left.\frac{\lambda_i}{\lambda_{i,T_{ref}}}\right|_{\alpha_{ref}} \quad \text{and} \quad A_\alpha|_{T_{ref}} = \left.\frac{\lambda_i}{\lambda_{i,\alpha_{ref}}}\right|_{T_{ref}} \quad (2)$$

The temperature-time shift factor, A_T and the cure-time shift factor, A_α, can be derived from the Williams–Landel–Ferry (WLF) framework,[5] along with relationships for dependence of T_g with the degree of cure (e.g., DiBenedetto equation[6]). In addition, the shift factor A_G, typically derived from the theory of rubbery elasticity,[7] captures the increase of the resin modulus with degree of cure, $G_0(\alpha)$. Simon et al.,[8] Prasatya et al.,[9] and Hojjati et al.,[10] have reported the use of the WLF framework (and DiBenedetto relationship) for calculation of cure-time and temperature-time shift factors, from dynamic shear and stress relaxation data measured during thermoset cure.

The assumption of thermo-chemo-rheological simplicity (employed in Refs. 8–10) does not apply for the entire duration of cure, involving transition in the relaxation behavior of the resin, from a viscous liquid at lower conversions ($\alpha < \alpha_{gel}$) to that of a rubbery gel, with additional relaxation mechanisms being introduced at gel point $\alpha = \alpha_{gel}$. Therefore, these experimental investigations,[8–10] and the associated cure-time-temperature shifts are restricted to the conversion-range $\alpha > \alpha_{gel}$. In this context, the cure-temperature-time superposition approach of Eom et al.,[1] while more empirical compared to that employed in Refs. 8–10, offers the cure-dependent shift factors for the entire conversion range and thus addresses the cure-dependent viscoelastic property development more comprehensively.

In this report, the evolution of cure induced stresses in the viscoelastic epoxy-amine thermoset resin from the study of Eom et al.[1] is simulated. The cure- and temperature-dependence of resin viscoelasticity is accounted for using the cure-temperature-time superposition approach proposed by Eom et al.[1] While this approach offers a more comprehensive description of the cure and temperature dependent resin property evolution, it also results in more complex expressions for description of the property evolution of the resin compared to those in Refs. 8–10. To facilitate faithful implementation of the model without any simplifying assumptions, multiphysics capabilities of a commercially available multiphysics FEM code offered by COMSOL[11] are employed. The simulated trends in viscoelastic stresses at different degrees of cure and temperatures are compared and contrasted with those obtained from two other equivalent material models—one involving a constant (cure- and temperature-independent) elastic modulus, and another involving a cure-dependent (but time-invariant) elastic modulus. Finally, the material models are implemented in the context of the cure of a thick thermoset resin part, to explore the combined effect of multiple phenomena—mold-part interaction, cure shrinkage strains, thermal strains, and the exothermic heat of reaction resulting in a two way coupling between heat transfer and chemical kinetics—on the evolution of residual stresses and springback

MATERIAL MODEL

In this section, the models for cure kinetics, and cure- and temperature-dependent viscoelastic behavior—that form the inputs for cure stress simulations presented subsequently—are described. These material models are for an epoxy-amine thermoset resin that has been characterized in detail by Eom et al.[1]

Cure Kinetics

The kinetics of the cure of this resin system is characterized by two distinct regimes: autocatalytic kinetics[12] at low conversions, and diffusion-limited nth order kinetics[13] at higher conversions. The autocatalytic model, valid in the conversion (α) range 0–0.5, is given as:

$$\frac{d\alpha}{dt} = (K_1 + K_2\alpha^{m_a})(1-\alpha)^{n_a} \quad (3)$$

$$K_1 = K_{01}\exp\left(\frac{-E_{01}}{RT}\right) \quad (4)$$

$$K_2 = K_{02}\exp\left(\frac{-E_{02}}{RT}\right) \quad (5)$$

where K_1 and K_2 are the temperature-dependent rate constants and m_a and n_a are temperature independent exponents. K_{01} and K_{02} are the temperature independent pre-exponential factors, and E_{01} and E_{02} are the activation energies associated with K_1 and K_2, respectively. R is the universal gas constant. These parameters, evaluated by Eom et al.,[1] are listed in Table I. The nth-order model, applicable at higher conversions ($\alpha > 0.5$) is given as:

$$\frac{d\alpha}{dt} = K_{eff}(1-\alpha)^n \quad (6)$$

In the above expression, n is the reaction order. K_{eff} is the overall effective reaction rate constant that takes into account both chemical and diffusion aspects that control the kinetics at high conversions.[14] K_{eff} is given as,

$$K_{eff} = \frac{K}{1+\exp[C(\alpha-\alpha_c)]} \quad (7)$$

$$K = K_0\exp\left(\frac{-E_0}{RT}\right) \quad (8)$$

Table I. Kinetic Parameters Calculated from Isothermal Cure of Epoxy-Amine, for Autocatalytic Model at Low Conversions, and for *n*th-Order Model at High Conversions (from Eom et al.[1])

Parameter	Value
Autocatalytic model (conversion range 0.0–0.5) [eq. (3)]	
K_{01} (1/s)	2.7321×10^5
K_{02} (1/s)	3.8231×10^5
E_{01} (J/mol)	7.2776×10^4
E_{02} (J/mol)	6.6934×10^4
m_a	1.07
n_a	2.43
Nth-order model (conversion range 0.5–1.0) [eq. (6)]	
K_0 (1/s)	29.10
E_0 (J/mol)	3.58×10^4
n	$-0.0403 \times T$ (K) $+19.48$
C	69
α_c	$0.0092 \times T$ (K) $- 3.14$

In the above expressions, K is the rate constant for chemical kinetics (non diffusion-controlled), C is a constant, and α_c is a critical conversion above which K_{eff} starts to deviate from K (diffusive effects come into play). K_0 and E_0 are the pre-exponential factor and the activation energy, respectively, associated with K. Eom et al.'s estimates[1] for these kinetic parameters for the epoxy-amine resin system are also listed in Table I. It is clear from Table I that the diffusion effects, as quantified by n and α_c, are strongly governed by the temperature of cure; at comparable degrees of cure, the stearic hindrance to diffusion of the reacting moieties is more significant at lower temperatures.

The simulated evolution of conversion as a function of time for isothermal cure of the epoxy-amine system is plotted in Figure 1 at four different isothermal cure temperatures, ranging from 155 to 170°C. It can be seen that diffusion effects prevent the cure reaction from reaching completion, and the final degree of cure shows progressive decrease with reduction of cure temperatures.

Experimental Cure-Temperature-Time Shift Calculations[1]

The viscoelastic properties of the curing thermoset resin were also studied by Eom et al.[1] using isothermal dynamic shear modulus measurements. The dynamic shear storage modulus at a given frequency, f, was taken to correspond to the relaxation modulus at time, $t = 1/f$ (cf. Ref. 3). The data for the relaxation moduli thus evaluated for the curing epoxy system were obtained for several degrees of cure, at a given cure temperature. The master curve of the viscoelastic response was then obtained at the reference conversion, by shifting the data at a given conversion on the logarithmic time axis until it neatly overlapped (or followed) the curve at the reference conversion. The logarithmic time difference between the real time t (corresponding to the data for the actual conversion) and the shifted (or reference) time ξ (corresponding to the location of the shifted data on the master curve) directly provided the logarithm of the shift factor (A_x): $\log A_x = \log t - \log \xi$. In other words:

$$A_x = \frac{t}{\xi} \tag{9}$$

At low conversions, the shift factors followed a logarithmic relationship with conversion. However, beyond the gel point ($\alpha_{\text{gel}} \sim 0.7$), the shift factors were observed to vary differently with conversion. This is indicative of the introduction of additional, and significantly different, relaxation mechanisms for the partially crosslinked gel that comes into existence post gel-point, compared to the relatively less crosslinked viscous resin that was present up to the onset of gelation. Also, up to $\alpha \sim 0.7$, Eom et al.[1] observed no variation in the magnitude of the shift factors (at a given conversion) with change in cure temperature. However, at higher conversions, the shift factors were seen to deviate, following the order of increasing cure temperature. Clearly, this is the impact of the choice of the reference conversion—equal to the maximum achievable degree of cure at a given temperature—which is a strong function of the diffusion effects following gelation, and hence the temperature of cure.

The observed trends in shift factors with respect to the degree of cure and the temperature were then fitted by Eom et al.[1] using two empirical shift models, to account for the two conversion regimes—before, and after, the onset of gelation. In the conversion range 0.0–0.7, only the cure-dependence of the shift factors needs to be accounted for, since they were observed to be temperature invariant:

$$\log A_x = C_1 \alpha + C_2 \tag{10}$$

The constants C_1 and C_2, evaluated by Eom et al. are listed in Table II. For the conversion range 0.7–1.0, in which gelation effects become dominant, Eom et al.[1] accounted for the dependency of the shift factor on both conversion and temperature, using the relationship shown in eq. (11).

$$\log A_x = A_{\text{gel}}\, H^{(\alpha-\alpha_{\text{gel}})} \left(\frac{\alpha_f - \alpha}{\alpha_f - \alpha_{\text{gel}}}\right)^{m_s} \tag{11}$$

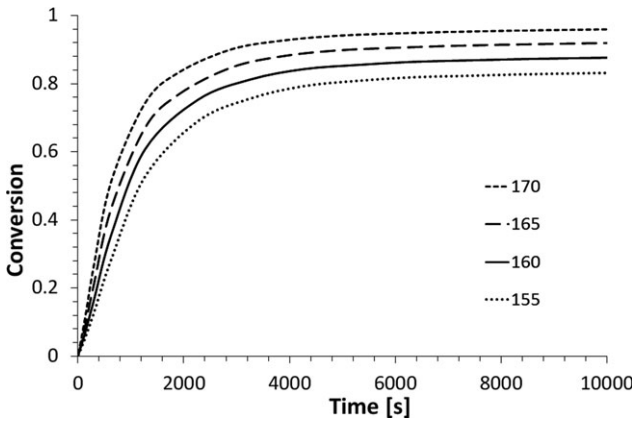

Figure 1. Calculated conversion of epoxy under isothermal curing conditions at four isothermal cure temperatures (°C, indicated in the legend).

Table II. Parameters for the Shift Factor Model for Cure-Temperature-Time Superposition, and for Generation of the Series Coefficients of the Linear Viscoelastic Model (from Eom et al.[1])

Parameter	Conversion: 0.0–0.7	Conversion: 0.7–1.0
Parameters for evaluation of time-cure-temperature shift factors		
C_1	30.6	-
C_2	−39.7	-
A_{gel}	-	−17.5
H	-	2
α_{gel}	-	0.7
α_f	-	0.0074 T (K) − 2.32
m_s	-	0.0346 T (K) − 14.23
Parameters for evaluation of series coefficients of the linear viscoelastic model		
G_∞	0.01	0.01
$G_{\tau 0}$	1.0×10^{-4}	1.0×10^{3}
G_{u0}	1×10^{4}	1.5×10^{8}
log(B)	0.1 T (K) − 62.8	0.332 T (K) − 149
n_p	10	22

With the boundary conditions,

$$\log A_x = A_{gel} \text{ at } \alpha = \alpha_{gel} \text{ and } \log A_x = 0 \text{ at } \alpha = \alpha_f \tag{12}$$

The above definition of shift factor, along with the definition of the temperature dependent parameters α_f and m_s, (refer to Table II) provides a complete description of both the conversion and temperature dependence of the viscoelastic response beyond gelation, α_{gel}, and also accounts for the temperature dependence of the limiting conversion α_f. These parameters, as evaluated by Eom et al. are also listed in Table II.

The shear stress relaxation master curve can be described using the generalized Maxwell model (with shifted times, ξ).

$$G_r(\xi, T_0) = G_\infty + \sum_{i=1}^{p} G_i \exp\left(\frac{-\xi}{\lambda_i}\right) \tag{13}$$

To account for the growth of G_0 with the degree of cure [refer to eq. (2)], Eom et al.[1] modeled the series coefficients of the relaxation spectrum using the phenomenological relationship shown in eqs. (14) and (15).

$$G_i = G_{\tau 0}\left(\frac{G_{u0}}{G_{\tau 0}}\right)^{D} \tag{14}$$

$$D = \left[1 - (1 - n_p)B\lambda_i\right]^{\frac{1}{1-n_p}} \tag{15}$$

$G_{\tau 0}$ is the minimum measurable relaxed modulus, G_{u0} is the unrelaxed modulus at the reference conversion, D is a parameter that determines the shape of the relaxation curve (which, in turn, is governed by the relaxation times, λ_i, of the resin), B is a temperature dependent material parameter, and n_p is a material constant. Eom et al.[1] employed different values for parameters in eqs. (14) and (15) in the conversion ranges before and after gelation. These parameters are listed in Table II. G_∞ was assigned a value of 0.01 Pa. Typically, the modulus would decay all the way to G_∞ within timescales of practical interest only at low degrees of cure (significantly below gel point) and temperatures substantially above the glass transition temperature of the thermoset.

Viscoelastic Model with Cure-Temperature-Time Shift

The viscoelastic material model implemented in the current simulation study captures all the features of the temperature-cure-time superposition model described in the earlier section, and has been implemented with the 34 relaxation time constants employed by Eom et al.[1] The viscoelastic response before gelation (corresponding to long times on the master curve) is described by employing 15 series coefficients with relaxation times ranging from 10^{18} to 10^{42} s (with one decade increments between 10^{18} and 10^{22} s, and two decade increments from 10^{22} to 10^{42} s). The response after gelation (corresponding to shorter times on the master curve) is described using 19 more series coefficients, with relaxation times ranging from 10^{-1} to 10^{17} s (with one decade increments). It should be noted that these relaxation time constants describe the relaxation master curve, at the limiting degree of cure at 170°C. Eom et al.[1] incorporated the extremely long relaxation times to accurately describe the intermediate rubbery plateau modulus and the subsequent complete relaxation of stresses. The 34-mode master relaxation spectra (G_i,λ_i) evaluated using eqs. (14) and (15), at four different temperatures, with the parameters in Table II, are plotted in Figure 2.

In the cure simulations employing the Eom et al.[1] model, the relaxation time of the resin at any given conversion, α, can be calculated by shifting the relaxation times at the reference conversion to the instantaneous conversion.

$$\lambda_{i\alpha} = A_x \lambda_i \tag{16}$$

The corresponding relaxation of shear modulus in real time, $G_r(t, T, \alpha)$, at different conversions can then be calculated by employing the shifted relaxation times, $\lambda_{i\alpha}$, as shown in eq. (17)

$$G_r(t, T, \alpha) = G_\infty + \sum_{i=1}^{p} G_i \exp\left(\frac{-t}{\lambda_{i\alpha}}\right) \tag{17}$$

The shear relaxation moduli at 170°C, calculated using eq. (17), are plotted in Figure 3 at different conversions. It is clear from this plot that the relaxation of stresses is fairly rapid even beyond the gel point conversion (0.7), and significant elasticity (the ability to hold the stresses) is developed only close to the limiting conversion. The bulk modulus, $\mathcal{K}$, and the elastic modulus, E of the curing resin are then calculated from the shear relaxation modulus, assuming a constant Poisson's ratio, v = 0.4, as shown below.[15]

$$E(t, T, \alpha) = 2(1 + v)G_r(t, T, \alpha) \tag{18}$$

$$\mathcal{K}(t, T, \alpha) = \frac{2(1 + v)G_r(t, T, \alpha}{3(1 - 2v)} \tag{19}$$

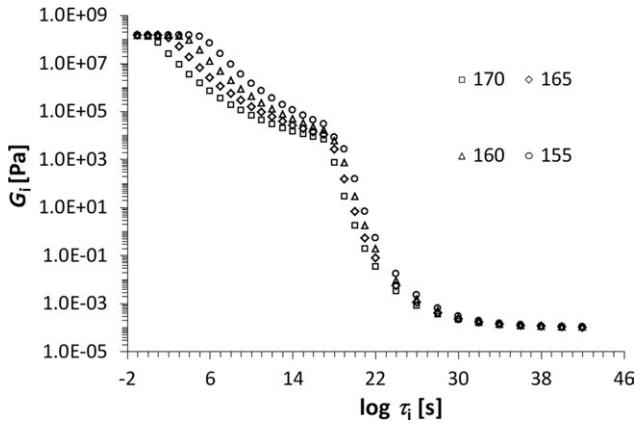

Figure 2. Series coefficients for the relaxation spectrum of the epoxy-amine resin as a function of the relaxation times at four different temperatures (°C, indicated in the legend).

Elastic Models

In addition to the cure- and temperature-dependent viscoelastic material model, two additional equivalent elastic material models were considered. The first was a cure- and temperature-dependent (but time invariant) elastic material model. In this model, the magnitude of the elastic shear modulus at any given degree of cure was set to the value of the viscoelastic shear relaxation modulus at extremely small times, at the same degree of cure.

$$G_{\text{cure\_elastic}}(T,\alpha) \equiv G_r(t = 10^{-12}s, T, \alpha) \tag{20}$$

In this model, while the cure dependence of G_0 is captured, its relaxation is not accounted for. $G_{\text{cure\_elastic}}$ is plotted against the degree of cure at 170°C in Figure 4. Comparing Figures 3 and 4, it is clear that $G_{\text{cure\_elastic}}$ at any given degree of cure is equivalent to the magnitudes of the shear relaxation moduli at the smallest times at the corresponding conversion. Consequently, the bulk and the Young's moduli are also cure dependent, but do not relax with time [and are calculated using $G_{\text{cure\_elastic}}(T,\alpha)$ analogously to eqs. (18) and (19), respectively].

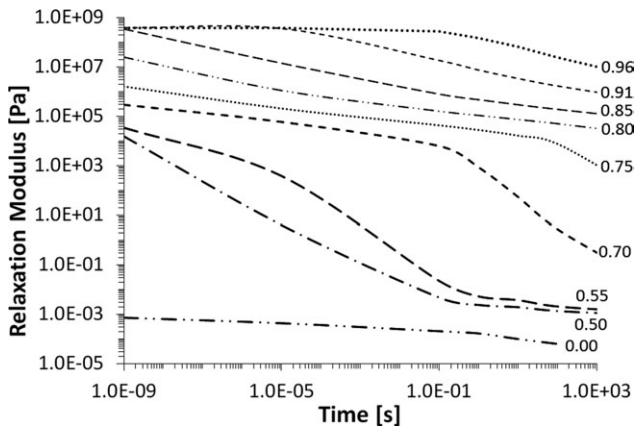

Figure 3. Shear relaxation modulus as a function of time at different conversions at 170°C.

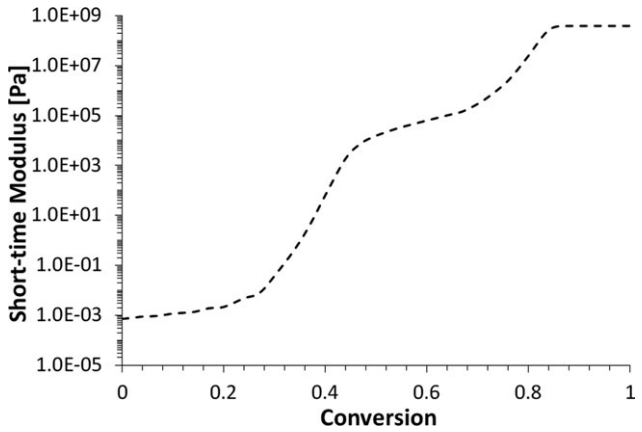

Figure 4. Evolution of shear relaxation modulus at extremely short times—equivalent to cure-dependent elastic modulus [eq. (20)]—as a function of degree of cure at 170°C.

Finally, a temperature-dependent (but time as well as cure invariant) elastic material model was considered. In this model, the magnitude of the elastic shear modulus at any given temperature was set to a value of the viscoelastic shear relaxation modulus at extremely small times at the maximum achievable degree of cure, α_f, corresponding to that temperature, as shown below.

$$G_{\text{const\_elastic}}(T) \equiv G_r(t = 10^{-12}\text{s}, T, \alpha = \alpha_f) \tag{21}$$

In this model, only the temperature dependence of the modulus of the fully cured resin (at α_f) is accounted for, and its relaxation is not accounted for. Consequently, the bulk and Young's moduli are also cure invariant and do not relax with time [and are calculated using $G_{\text{const\_elastic}}(T)$ analogously to eqs. (18) and (19), respectively].

MATERIAL MODEL IMPLEMENTATION

The cure stress simulations using the cure-kinetics and the time-cure-temperature shift scheme described in earlier sections, were implemented for the viscoelastic and elastic material models (described in the foregoing) in COMSOL Multiphysics®—Version 3.5a. The additional resin parameters required for these simulations are listed in Table III, and were assigned typical values for thermoset epoxy resins (e.g., Ref. 16, 17). The viscoelastic model implementation in COMSOL®, summarized below, was verified using two model load case scenarios. Finally, we describe the implementation of the material models in the context of the cure of a thick thermoset resin part, to explore the combined impact of global constraints, reaction exotherm, and spatial variation in temperature and degree of cure on the evolution of residual stresses and springback.

COMSOL Multiphysics® Implementation of Viscoelastic Model[11]

The generalized Maxwell model shown in eq. (17) may be expressed as a Prony series, as shown in eq. (22).

$$G_r(t,T,\alpha) = G_0\left[\mu_\infty + \sum_{i=1}^{p}\mu_i \exp\left(\frac{-t}{\lambda_{i\alpha}}\right)\right] \tag{22}$$

Table III. Magnitudes of Relevant Thermal, Chemical, and Mechanical Properties of the Resin Employed for Calculation of Cure-Induced Stresses

Density (kg/m^3)	ρ	1.2×10^3
Specific heat (J/kg K)	C_P	1.25×10^3
Heat of reaction (J/mol)	$\Delta H_{reaction}$	100,000
Thermal conductivity (W/m K)	k	0.2
Poisson's ratio	ν	0.4
Coefficient of thermal expansion (ppm/K)	χ	100
Specific volumetric shrinkage during cure (%)	$\Delta V_{shrinkage}$	6.0

These values are typical of epoxy resins (e.g., Refs. 16 and 17) and are therefore assumed to apply to the epoxy-amine system of Eom et al.[1] These properties are not reported in Eom et al.

In the above equation, the coefficient μ_i can be considered to be the relative stiffness (G_i represents the absolute stiffness) of the spring in branch i of the generalized Maxwell model.[4]

$$\mu_i \equiv \frac{G_i}{G_0} \; ; \; \mu_\infty \equiv \frac{G_\infty}{G_0} \tag{23}$$

$$\mu_\infty + \sum_{i=1}^{p} \mu_i = 1 \tag{24}$$

In the COMSOL Multiphysics® implementation of viscoelasticity, the viscous portion of the deformation is set to be incompressible, and any volume change associated with stress relaxation is purely elastic.[11] This assumption, along with the representation of the relaxation modulus in eq. (22) leads to the development of the differential equation form of the viscoelastic model—shown in eqs. (25)–(39), along with eq. (24). The overall stress, σ, has contributions from an isotropic (pressure) component, p, and a deviatoric stress component, τ.

$$\sigma = \tau - p\mathbf{I} \tag{25}$$

The isotropic component of the stress is defined in terms of the bulk modulus, $\mathcal{K}$, and isotropic strains:

$$p = -\mathcal{K} \cdot \mathrm{trace}(\varepsilon) = -\mathcal{K} \cdot (\varepsilon_{11} + \varepsilon_{22} + \varepsilon_{33}) \tag{26}$$

The deviatoric strains are defined as:

$$\varepsilon_{\mathrm{deviatoric}} = \varepsilon - \frac{1}{3}\mathrm{trace}(\varepsilon) \cdot \mathbf{I} \tag{27}$$

The components of the deviatoric part of the stress tensor, τ, and the deviatoric strains are related through the generalized Maxwell model, by introducing the variable q_i, that is equivalent to the extension of the spring in branch i of the generalized Maxwell model, as shown in eqs. (28) and (29).

$$\tau = 2G_0\left(\mu_\infty \varepsilon_{\mathrm{deviatoric}} + \sum_{i=1}^{p} \mu_i q_i\right) \tag{28}$$

$$\dot{q}_i + \frac{1}{\lambda_i} q_i = \dot{\varepsilon}_{\mathrm{deviatoric}} \tag{29}$$

Model Load Cases for Verification of Viscoelastic Model Implementation

The 2D geometry employed for the model load case simulations is shown in Figure 5(a,b). All the simulations were carried out under isothermal conditions. The coefficient of thermal expansion was assumed to be zero in all simulations, thereby not accounting for any thermal strains. Assuming the body forces to be negligible, the momentum balance equation:

$$\nabla \cdot \sigma = 0 \tag{30}$$

was implemented in the geometry shown in Figure 5 using the plane strain approximation, in which the geometry is considered infinitely long in z- (3-) direction, thereby making it possible to ignore any normal or shear strains in that direction:

$$\varepsilon_{33} = \varepsilon_{23} = \varepsilon_{13} = 0 \tag{31}$$

Two different loading scenarios were investigated to study the response of the viscoelastic and the elastic material models. The first scenario involved the near instantaneous application of a finite strain and simulating the state of purely mechanical stresses while the finite strain is held constant. This constitutes a typical stress relaxation experiment for a viscoelastic material. The second scenario involved simulation of the evolution of stresses due to chemical crosslink induced shrinkage in a fully constrained resin undergoing isothermal cure.

Mechanical Stress Evolution in Step-Strain Experiments

In this set of isothermal simulations, the geometry was assigned a constant and uniform temperature (T_{ref}). The chemical kinetics was not solved for; instead, the degree of cure was *a priori* assigned. At this assigned degree of cure, and T_{ref}, the time-cure-temperature shift factors were calculated using either eq. (10) or eqs. (11) and (12) (depending on whether $\alpha < \alpha_{\mathrm{gel}}$ or $\alpha \geq \alpha_{\mathrm{gel}}$). The relaxation spectrum was calculated using eqs. (14) and (15), and employing the parameters given in Table II (once again, the choice of parameters was depending on whether $\alpha < \alpha_{\mathrm{gel}}$ or $\alpha \geq \alpha_{\mathrm{gel}}$). The viscoelastic shear relaxation modulus was then evaluated by employing the relaxation spectrum and the shift factors, using eqs. (16) and (17). The cure dependent elastic modulus, at the assigned degree of cure, was then set to a constant value as shown in eq. (20).

For this set of simulations, the cure-induced shrinkage strain was ignored, and only purely mechanical strains were considered. As shown in Figure 5(a), an overall mechanical tensile strain of 0.05 was imposed on the longer dimension of the geometry using a rapid constant-velocity strain ramp within 0.005 s, and then this strain was maintained for the remaining portion of the simulation.

$$\varepsilon_{11} = \varepsilon_{11}^{\mathrm{Mechanical}} \begin{array}{ll} = 0 & (t = 0\mathrm{s}) \\ = 0.05 & (t \geq 0.005\mathrm{s}) \end{array} \tag{32}$$

The evolution of mechanical stresses in the step-strain experiments were simulated at four different degrees of conversion above the gel point at 170°C, and at three different temperatures at a conversion of 0.8.

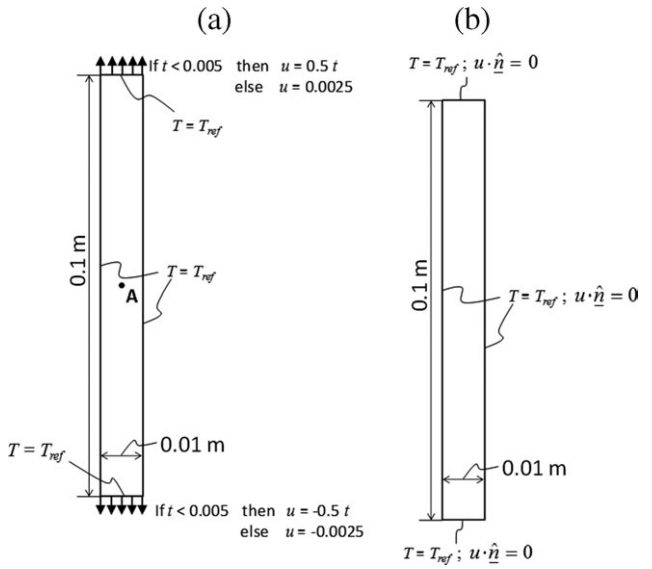

Figure 5. Schematic showing the geometry (not to scale) and thermomechanical boundary conditions for the simulation of (a) development of purely mechanical stresses following rapidly imposed extensional strain in the resin at a fixed degree of cure at a given temperature, and (b) the evolution of stresses due to chemical crosslink induced shrinkage in a fully constrained resin undergoing isothermal cure.

The simulated stresses associated with rapid imposition of extensional strain at 170°C are plotted for three different degrees of cure in Figure 6. In this figure, the response of the material with cure-dependent elastic modulus is compared with that of the viscoelastic material. For both material models, the magnitudes of stresses at equivalent strains increase with increasing degree of cure. For the cure-dependent elastic material model, the stresses monotonically increase with time for the duration of the application of the constant velocity deformation up to 0.005 s. After 0.005 s, as the strain is held constant, the stresses also remain constant. For this material model, the responses at conversions of 0.95 and 0.9 are exactly the same, and the stress transients perfectly overlap; this can be explained by inspecting Figures 3 and 4 that show a nearly constant cure dependent modulus of the material at extremely small times after a conversion of 0.88 (indicating vitrification).

The use of viscoelastic material model results in significantly different trends. After 0.005 s, as the imposed strain is held constant, the stresses relax to values significantly lower than those observed at 0.005 s. The relaxation of stresses relative to the initial stress value becomes progressively more significant at lower degrees of cure. This is consistent with the significantly smaller relaxation times of the crosslinking gel at a conversion of 0.8 compared to the fully cured material at a conversion of 0.95 (refer to Figure 3). The build-up of stresses during the deformation phase, up to 0.005 s, is significantly lower than that observed with the cure-dependent elastic material model. The stress response at conversions of 0.9 and 0.95 are very different, while the response at these two conversions for the elastic material showed perfect overlap. This is consistent with the fact that even though the relaxation moduli at extremely short times are very similar at the conversions of 0.88 or higher, the long-time relaxation behaviors are very different, as observed in Figure 3. More importantly, the stresses start relaxing even during the initial 0.005 s when the deformation is still being imposed. This behavior is most pronounced at the lower conversions, because the relaxation times of the resin at these conversions are smaller than even the short timescale of strain imposition. The initial time response of the viscoelastic material model predictions closely follows that of the elastic material model only at the highest conversion of 0.95.

The stress relaxation response for the viscoelastic material model, at a conversion of 0.8, is plotted in Figure 7 at three different temperatures. It is clear from Figure 7 that as the temperature is lowered, the magnitude of stresses increase in both the strain build up phase (up to 0.005 s) and the constant strain phase (beyond 0.005 s). During the strain build-up phase, the relaxation of stresses is least pronounced at the lowest temperature. At all times, the resin stresses at 160°C are nearly an order of magnitude higher than that at 170°C.

Chemical Shrinkage Stresses During Isothermal Cure in a Fully Constrained Geometry

This is a hypothetical scenario aimed at exploring the evolution of purely crosslink-shrinkage induced residual stresses in the resin in the absence of any mechanical strains. Clearly, at low degrees of cure substantially below the gel point, the state of completely constrained resin is not practically achievable, since the viscous resin has a tendency to flow. However, the cure-dependent elastic and viscoelastic material models indirectly account for the viscous nature of the resin through assignment of extremely low elastic moduli and extremely small relaxation time constants, respectively.

In this isothermal simulation, the geometry was assigned a constant and uniform temperature of 170°C (T_{ref}). The chemical kinetics was solved for at 170°C using eqs. (3)–(8). At any instantaneous degree of cure, and T_{ref}, the time-cure-temperature shift factors were calculated using either eq. (10) or eqs. (11)

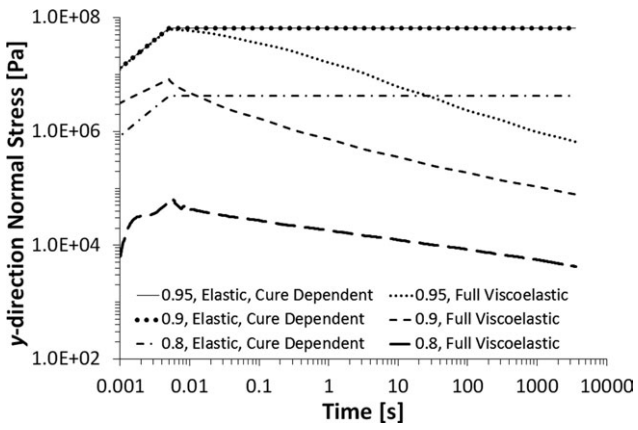

Figure 6. Simulated transients of purely mechanical stresses following rapidly imposed y-direction extensional strain (within 0.005 s) in the resin at a temperature of 170°C, and three different degrees of cure; comparison of trends obtained for viscoelastic, and cure-dependent elastic material models.

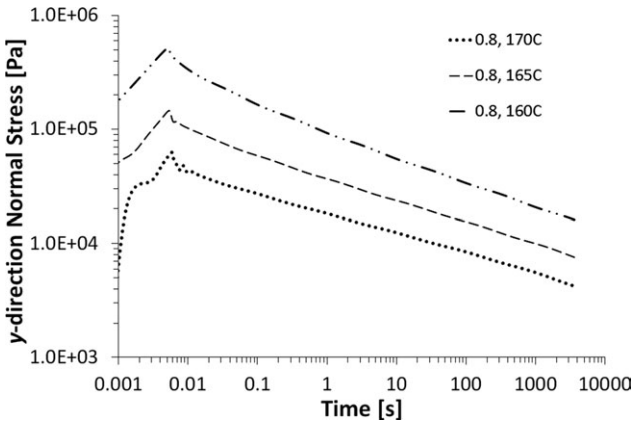

Figure 7. Simulated transients of purely mechanical stresses, following rapidly imposed *y*-direction extensional strain (within 0.005 s) in the resin at a degree of cure of 0.8, and three different temperatures, using the viscoelastic material model.

and (12) (depending on whether $\alpha < \alpha_{gel}$ or $\alpha \geq \alpha_{gel}$). The relaxation spectrum was calculated using eqs. (14) and (15), and employing the parameters given in Table II (once again, the choice of parameters was depending on whether $\alpha < \alpha_{gel}$ or $\alpha \geq \alpha_{gel}$). The viscoelastic shear relaxation modulus was then evaluated by employing the relaxation spectrum and the shift factors, using eqs. (16) and (17). The cure dependent elastic modulus, was allowed to evolve with the degree of cure as shown in eq. (20), and as seen in Figure 4.

For this simulation, the geometry was fully constrained at all the edges, thereby setting the mechanical strains to zero [refer to Figure 5(b)],

$$n \cdot \boldsymbol{u} = 0 \quad \text{along all the edges of the domain} \tag{33}$$

On the other hand, an overall volumetric shrinkage of 6% was considered for the fully cured material at 170°C: $\Delta V_{\text{shrinkage}} = -0.06$. In an unconstrained geometry, this would result in isotropic shrinkage strains, as shown below (e.g., Ref. 17).

$$\varepsilon_{ij}^{\text{Shrink}} = (\sqrt[3]{1 + \Delta V_{\text{shrinkage}}} - 1)\delta_{ij} \tag{34}$$

However, in a fully constrained geometry, it would result in a tensile hydrostatic state of stress, incorporated in the pressure term [refer to eq. (26)] as shown below:

$$p = -\mathcal{K} \cdot \{\text{trace}(\varepsilon) - 3\varepsilon_{ij}^{\text{Shrink}}\} \tag{35}$$

The evolution of the isotropic crosslink shrinkage stresses can then be calculated by equally distributing the overall volumetric shrinkage over the entire cure.

$$p(\alpha) = -\mathcal{K} \cdot \{\text{trace}(\varepsilon) - 3\varepsilon_{ij}^{\text{Shrink}}\alpha\} \tag{36}$$

The evolution of chemical shrinkage stress over the duration of cure, simulated at 170°C, has been plotted for the three material models, in Figure 8. The tensile nature of the hydrostatic stresses in the constrained geometry due to chemical-crosslink induced shrinkage is seen from the positive values for stresses at all times. From eq. (36), it can be seen that the evolution of chemical crosslink induced shrinkage would closely follow the degree of cure transients (refer to Figure 1). With a constant elastic modulus, the evolution of shrinkage strains or stresses would also display the same monotonic evolution as the degree of cure—as evidenced in the constant elastic material model response plotted in Figure 8. The evolution of stresses in a material with cure dependent elastic material model trails that in a constant elastic modulus material, because the modulus starts out as G_∞ at $t = 0$, and progressively increases with the degree of cure. However, once the modulus has evolved completely at high degrees of cure, the magnitude of stresses is the same as that in a constant-elastic-modulus material. Thus, upon achievement of the maximum degree of cure, there is no difference in the stress response of the material models involving a constant elastic modulus or a cure-dependent elastic modulus.

In sharp contrast to the two elastic material models, the viscoelastic material model results in significantly slower buildup of stresses and lower magnitude of stresses even upon achievement of the maximum degree of cure. Two regimes of stress relaxation can be noted. The first phase of stress relaxation occurs even as the degree of cure is increasing. In the initial stages, at low degrees of cure, the viscoelastic response is characterized by low moduli and extremely small relaxation times, leading to rapid relaxation of stresses to a very low magnitude (G_∞). Up to the gel point the resin behaves as a viscous liquid, and does not develop significant magnitude of stresses. The stresses build up slowly once high degrees of cure are achieved beyond 2500 s (after the onset of gel point). The second phase of slow relaxation of stresses occurs beyond 10,000 s, when the increase in the degree of cure is relatively slow, and additional shrinkage strains are not accumulated, while at the same time the relaxation times of the resin do not get substantially altered. This slow relaxation of stresses in a completely cured resin would typically approach the rubbery plateau modulus at extremely long times.

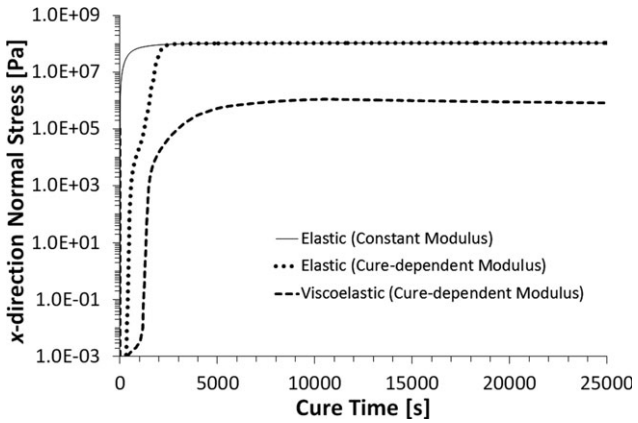

Figure 8. Simulated evolution of stresses due to chemical crosslink induced shrinkage in a fully constrained resin undergoing isothermal cure at 170°C; comparison of trends obtained for viscoelastic, cure-dependent elastic, and constant elastic material models.

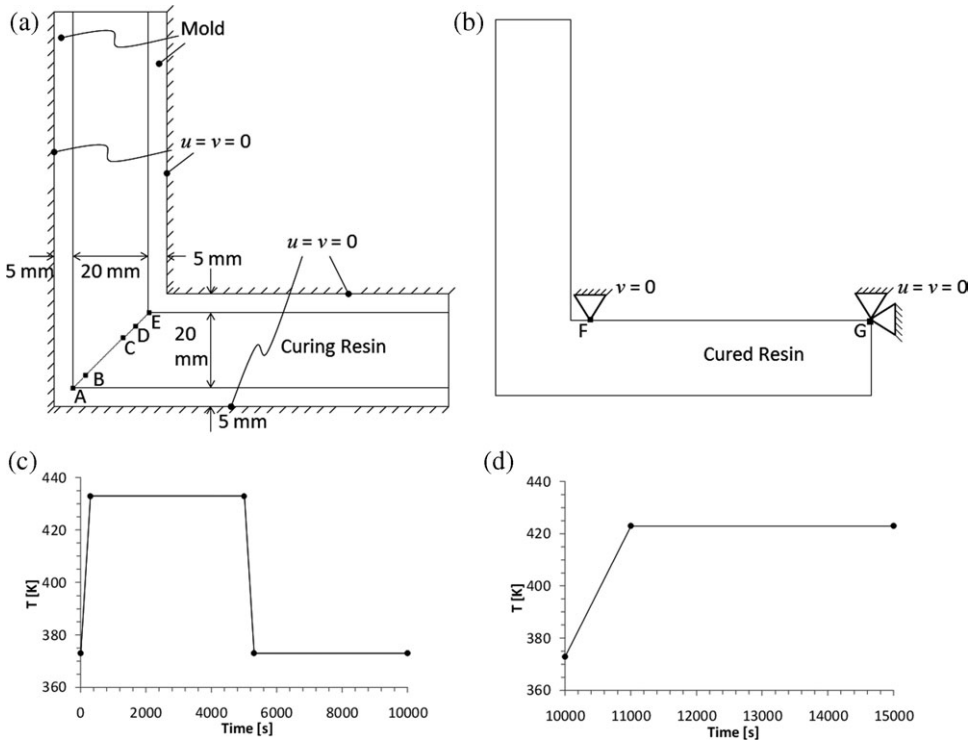

Figure 9. The geometry, and mechanical boundary conditions, for simulation of the evolution of residual stresses during (a) the cure of a thick thermoset elbow geometry constrained between two structural steel molds, followed by (b) partially constrained heating of the cured thermoset part under point constraints. The corresponding thermal cycles imposed on all the exposed edges of the geometry are shown in (c) and (d), respectively. The evolution of temperature, cure, and stresses are investigated along the diagonal traversing the thickest portion of the thermoset resin in the elbow geometry at the points A (0,0), B (0.0025,0.0025), C (0.01358,0.01358), D (0.0175,0.0175), and E (0.02, 0.02) [refer to Figure 9(a)].

Of course the long-time relaxation of stresses at limiting conversion is also driven by the high temperature (170°C); the stress relaxation would be substantially slower upon cool down to room temperature. It is clear that accounting for the viscoelastic behavior of the resin results in significant reduction in the simulated stress build up during application of strains, and additional long time relaxation even after achievement of complete conversion.

As mentioned earlier, in this simulation, the overall volumetric shrinkage has been equally distributed over the entire cure [eq. (36)]. On the other hand, the model developed by Adolf and Chambers[18] assumes that effective shrinkage accumulates only after branches develop into effective crosslinks, i.e., after onset of gelation. Predictions based on gel-point conversion model may therefore provide relatively larger estimates of residual stresses based on shrinkage since onset of shrinkage strains is assumed to occur after the modulus of the resin has developed into the rubbery region (with relatively longer relaxation times). The choice of the appropriate shrinkage evolution model requires characterization of the evolution of shrinkage with the degree of cure.

Cure-Induced Residual Stresses and Springback in Thick Sections: A Case Study on Thick Elbow Section

Residual stress development and shape distortions in thick thermoset sections are often further influenced by large temperature gradients across the thickness. Cure reactions are exothermic in nature, with heats of reaction reaching close to 500,000 J/kg for some vinyl ester resins (e.g., Ref. 19). During curing the mold surface temperatures are controlled, but the temperatures within the core are governed by the heat generation and transfer. In thin thermoset parts, the large exposed surface area to volume ratio allows the extraction of the cure exothermic heat despite the low thermal conductivity of the thermoset resins. However in thick sections, the exothermic heat cannot be extracted easily due to the low exposed surface area to volume ratio and large thermal mass of the resin, and the temperature at the core can substantially overshoot that at the surface.[20] Such large gradients in temperature result in equally large gradients in the degree of cure (and the associated resin shrinkage, modulus, and glass transition temperature) along the thickness of the section. To understand these effects, the cure-dependent elastic and viscoelastic models, discussed earlier, are implemented in the context of the cure of thick sections, to explore the combined effect of multiple phenomena—mold-part interaction, cure shrinkage strains, thermal strains, and the exothermic heat of reaction resulting in a two way coupling between heat transfer and chemical kinetics—on the evolution of residual stresses and springback.

Problem Definition

The geometry and thermomechanical conditions for this simulation involving a hypothetical scenario associated with the cure of a thick right-angled elbow section are depicted in Figure 9.

Table IV. Relevant Thermal and Mechanical Properties of Structural Steel[21]

Density (kg/m^3)	ρ	7.85×10^3
Specific heat (J/kg K)	C_P	475
Thermal conductivity (W/m K)	k	44.5
Young's modulus (GPa)	E	200
Poisson's ratio	ν	0.33
Coefficient of thermal expansion (ppm/K)	χ	12.3

This simulation is implemented in two stages: (I) the first stage involves the cure of a 2-cm thick thermoset in the shape of a right-angled elbow, with the longer (outer) dimension of each arm 10 cm, under constraint between two 5-mm thick structural steel molds [Figure 9(a)] —to study the evolution of residual stress; (II) the second stage involves the re-heating of the cured elbow geometry (after removal of the molds) under point constraints [Figure 9(b)]—to explore spring-back effects. The thermal cycle for the first phase, with duration of 10,000 s, is shown in Figure 9(c), and is imposed on all the external boundaries of the geometry shown in Figure 9(a). The thermal cycle involves a heating phase from 373 to 433 K within 300 s, an isothermal hold at 433 K for the next 4700 s, cool down to 373 K within the next 300 s, and a second isothermal hold at 373 K for the next 4700 s. The heating cycle for the second phase, for a subsequent duration of 5000 s, is shown in Figure 9(d), and is imposed on all the edges of the cured resin shown in Figure 9(b). This thermal cycle involves a heating phase from 373 to 423 K in 1000 s, followed by an isothermal hold at 423 K for the next 4000 s. As shown in Figure 9(a), during the first thermal cycle, the exposed long edges of the structural steel molds are fixed. The short edges of the mold, along the mold thickness, and the exposed surfaces of the resin are free to deform. The perfect contact (equal displacement) is imposed on the internal boundaries involving the resin-mold interface. During the second heating cycle, the mold constraints are removed, and the cured elbow is constrained at only two points [points F and G, in Figure 9(b)] to prevent any solid body rotation. In both phases of the simulation, any impact of the resin viscosity and gravity on the flow-induced resin rearrangement and convective heat transfer are ignored. The relevant thermomechanical properties of the structural steel mold are listed in Table IV (adopted from Ref. 21).

The cure kinetics is described by eqs. (3)–(8), along with the parameters listed in Table I. The cure kinetics simulation is carried out only within the resin subdomain. The conductive heat transfer within the structural steel molds is defined as shown below.

$$\rho C_P \frac{\partial T}{\partial t} - \nabla \cdot (k \cdot \nabla T) = 0 \qquad (\textbf{mold}) \tag{37}$$

In the above equation, ρ, C_p, and k are, respectively, the density, specific heat, and thermal conductivity of the material. The conductive heat transfer within the curing resin accounts for the heat generation due to the exothermic heat of reaction, as shown below.

$$\rho C_P \frac{\partial T}{\partial t} - \nabla \cdot (k \cdot \nabla T) = \rho \Delta H_{\text{reaction}} \frac{d\alpha}{dt} \qquad (\textbf{resin}) \tag{38}$$

As seen above, the rate of heat evolution during cure is governed by the overall enthalpy of the cure reaction ($\Delta H_{\text{reaction}}$) and the instantaneous rate of reaction. The heat generation term on the right hand side provides a two-way coupling between the heat and the mass balances—the progress of cure results in generation of exothermic heat, which in turn increases the reaction rates. The magnitude of $\Delta H_{\text{reaction}}$ employed for this simulation is typical of epoxy resins (e.g., Ref. 17) and is listed in Table III.

The structural mechanics problem definition, involving plane strain approximation, is shown in eqs. (30) and (31). In the first phase involving the mold-constrained cure of the resin, the momentum balance [eq. (30)] addresses the development of residual stresses in the curing resin due to the differential thermal strains between the structural steel mold and the thermoset, and also due to chemical shrinkage strains. In the second phase, the momentum balance addresses the combined impact of the residual stresses developed in the first stage, and the additional thermochemical strains, on the springback behavior of the cured resin heated under point constraints. The coefficients of linear thermal expansion (χ) of the epoxy resin (representative value for epoxies (e.g., Ref. 16), and the structural steel[21] are listed in Tables III and IV, respectively. The evolution of the isotropic (hydrostatic) stresses due to thermal strains in the structural steel molds, is incorporated in the pressure term [refer to eqs. (25) and (26)] as shown below:

$$p(T) = -\mathcal{K} \cdot \{\text{trace}(\varepsilon) - 3\chi(T - T_{\text{ref}})\} \qquad (\textbf{mold}) \tag{39}$$

For this analysis, the reference temperature for thermal strains was taken to be 373 K. On the other hand, the isotropic (hydrostatic) stresses generated in the thermoset resin are a combination of thermal stresses and those arising due to chemical shrinkage, and the corresponding isotropic pressure term [refer to eqs. (25) and (26)], can be expressed as shown below.

$$p(T, \alpha) = -\mathcal{K} \cdot \{\text{trace}(\varepsilon) - 3\varepsilon_{ij}^{\text{Shrink}}\alpha - 3\chi(T - T_{\text{ref}})\} \qquad (\textbf{resin}) \tag{40}$$

The details of implementation of this simulation are briefly described in the Appendix.

Evolution of Temperature, Degree of Cure, and Residual Stresses

The temperature and degree of cure transients in the thermoset resin during the first cure cycle within the mold—at the points A–B–C–D–E along the diagonal traversing the thickest portion of the thermoset resin in the elbow geometry [refer to Figure 9(a)]—are shown in Figure 10(a,b), respectively. At points A and E, which are in contact with the corners of the structural steel molds, the temperature transients mimic the imposed thermal cycle on the outer surfaces of the molds [Figure 10(a)]. Because of the high thermal conductivity of structural steel, the molds offer insignificant thermal barrier to heat transfer into

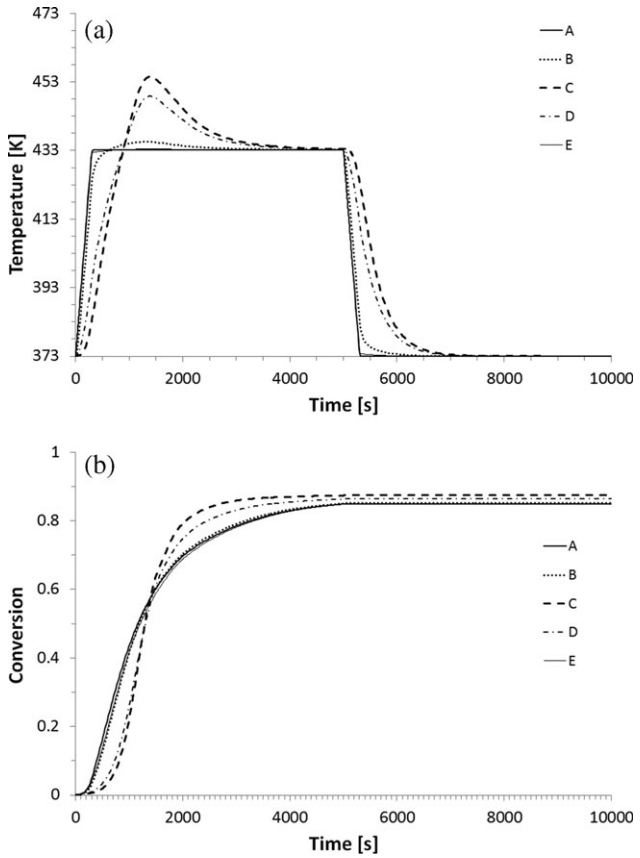

Figure 10. The simulated evolution of (a) temperatures, and (b) degrees of cure, in the thermoset resin at the points A–B–C–D–E [refer to Figure 9(a)] during the first cure cycle within the mold for 10,000 s.

the resin. The degree-of-cure transients also evolve similarly at points A and E [Figure 10(b)].

By virtue of the right angled elbow geometry, the conductive heat transfer from the resin to the two proximal mold walls is enhanced in the vicinity of the location A, whereas a major portion of conductive heat transfer at the location E, at the re-entrant (convex) inner mold corner, occurs towards the resin. The thermal mass of the resin and the thermal gradients within the resin—further enhanced by the exothermic heat of the cure reaction—are therefore significantly higher in the vicinity of point E as compared to the vicinity of point A. At location B, the enhanced conductive heat transfer to the proximal mold walls in the vicinity of corner A results in a quick rise of temperatures in the initial heating phase, only minor deviations from the isothermal hold temperature due to rapid removal of exothermic reaction heat, and a cool-down ramp similar to that imposed on the mold walls [Figure 10(a)]. Consequently, the degree of cure transient at B is also very similar to those at locations A and E [Figure 10(b)].

By contrast, the temperature rise at locations C and D, which are closer to the re-entrant corner E, significantly trails the mold heating cycle [Figure 10(a)]. The progress of cure is also substantially slower at points C and D, compared to A, B or E, for the initial 1000 s [Figure 10(b)]. However, as cure progresses, the exothermic heat evolving at C and D cannot be dissipated fast enough (owing to the thickness of the part and the poor conductive heat removal to the mold walls in the vicinity of E) and the temperature at the these points rises above that at the mold surface [Figure 10(a)]. This in turn leads to faster reaction at these locations and therefore more heat due to the reaction exotherm. At the timescales corresponding to the temperature maximum [cf. Figure 10(a)] the conversion at the locations C and D also shows a rapid increase and exceeds that at the surfaces [Figure 10(b)]. The maximum temperatures due to the exothermic heat of reaction ($\sim$20°C above the mold temperatures) are achieved at the location C, which is not in the exact middle of the thickness of the elbow, but nearer to the re-entrant corner (point E). During the cool-down period starting at 5000 s, the temperature drop is also slowest at the location C. From a comparison of Figure 10(a,b), it can be seen that the final degree of cure achieved at the end of the cycle at any given location is clearly a function of the maximum temperature achieved at that location. However, since the exothermic temperature rise lasts only for a small portion of the first isothermal hold, as seen in Figure 10(a), the final degrees of cure at the various points are still dominated by the diffusion controlled limiting conversion corresponding to the hold temperature [eqs. (6)–(8)], and do not show a very large spread.

The thermochemical residual stress transients within the curing thermoset resin were estimated by the simultaneous FE solutions of the kinetic model, the heat balance, and the momentum balance (the implementation details are laid out briefly in the Appendix). In Figure 11(a), the transients of the maximum principal stress during the first cure cycle within the mold, estimated for an elastic resin with a cure- and temperature-dependent elastic modulus [refer to eq. (20)] have been plotted at the points A–B–C–D–E [cf. Figure 9(a)]. At location A, the stresses start building up around 2000 s, which corresponds to the achievement of the gel point conversion ($\alpha = \alpha_{gel} = 0.7$) of the thermosetting resin. Prior to 2000 s, at degrees of cure substantially below the gel point, the magnitudes of moduli are quite insignificant to result in any stresses owing to thermal expansion due to temperature increase in the first 300 s [cf. Figure 10(a)] or the development of shrinkage strains up to the gel point. As limiting conversion is attained, the magnitude of stress stabilizes, up to 5000 s. Starting at 5000 s, during the cool-down phase, the stresses increase once again, due to the onset of constrained thermal shrinkage during cool-down, and stabilize at the final value.

While the location A is subjected to the constraining effects of the mold (owing to the concave corner, and also enhanced conductive heat transfer from the resin to the mold) at the locations C, and D, the resin is relatively unconstrained (the locations B and E may be considered partially constrained by the mold corners); therefore the development of stresses at C and D is not only impacted by the instantaneous temperature and degree of cure, but also the spatial gradients in temperature and conversion in the vicinity of these points. Consequently, the

Applied Polymer SCIENCE

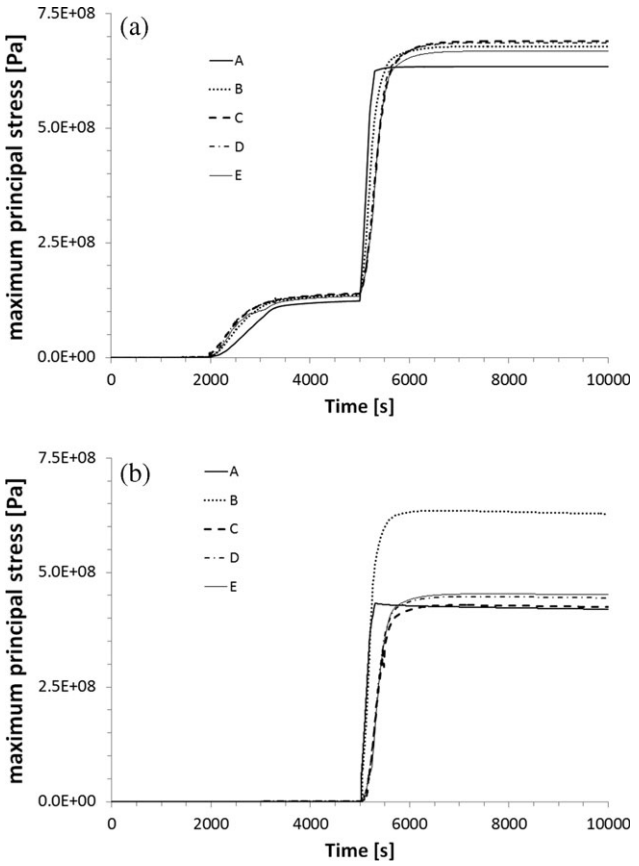

Figure 11. The estimated transients of in the maximum principal stress at the points A–B–C–D–E [refer to Figure 9(a)], obtained by employing (a) a linear elastic material model with a cure- and temperature-dependent resin elastic modulus, and (b) a viscoelastic material model with cure- and temperature-dependent resin relaxation spectrum.

evolution of stresses at these locations slightly deviates from that at points A, B, and E as seen in Figure 11(a).

For an elastic resin, however, the differences in the evolution of stress transients notwithstanding, the final state of stress distribution within the bulk of the section is governed primarily by the final state of distribution of the degree of cure and temperatures within the resin. Since the spatial distribution of the final degree of cure at 10,000 s is not very broad [refer to Figure 10(b)], and the temperatures are spatially invariant, the distribution of stresses within the bulk, as demonstrated by the magnitudes of the maximum principal stresses at points B, C, and D, is also relatively narrow.

In Figure 11(b), the evolution of the maximum principal stresses estimated for a linear viscoelastic resin with a cure- and temperature-dependent relaxation spectrum have been plotted at the points A–B–C–D–E during the first cure cycle within the mold. In the viscoelastic scenario, all the thermo-chemo-mechanical mechanisms underlying the development of residual stresses discussed in the context of the elastic material model apply, but additionally, the viscoelastic relaxation of stresses also comes into effect. Comparison of Figure 11(a,b) reveals, consistent with the earlier discussion on model load-case scenarios, that accounting for viscoelastic stress relaxation results in relatively lower estimates for stresses compared to those obtained with the linear elastic material model. Even after the onset of gel point (between 2000 and 5000 s) the stresses in the viscoelastic material undergoing cure are insignificant since the relaxation times continue to remain fairly small up to very close to the limiting conversions. Relaxation of the stresses within the core (locations C and D) during the isothermal hold up to 5000 s is further expedited by the high temperatures at the core due to the exothermic heat. After 5000 s, since the locations C and D cool down much slower than the mold [cf. Figure 10(a)] these locations experience significant dwell-times at temperatures which are substantially higher than the mold temperatures; this allows quicker relaxation of stresses brought about by thermal shrinkage, and slower build-up of stresses. However, at the points A and B, since the cool-down occurs at nearly the same rate as that at the mold, the stresses do not relax as rapidly, and therefore build up faster to a significantly greater value compared to the stresses at C and D (and comparable to that estimated with the elastic material model). Therefore, at the end of cure, even though the temperatures are spatially invariant, and the distribution of final degree of cure is not very broad, the distribution of stresses within the bulk, as demonstrated by the magnitudes of the maximum principal stresses at points B, C, and D, is quite broad, owing to the significantly different thermal history at point B compared to those at points C and D.

The spatial distribution of the maximum principal stresses—estimated with the elastic material model and the linear viscoelastic material model—at the end of the first cure cycle (10,000 s) are shown in the form of contour maps in Figure 12(a,b), respectively. Figure 12(a,b) also shows the deformations brought about by the cure of the resin. The edges of the thermoset in contact with the mold are for all practical purposes fully constrained due to the large difference between the coefficients of linear thermal expansion of the mold and the resin. However, the two exposed edges of the curing resin, which are constrained by the steel molds at their end points alone, deform into a concave arc as a result of the shrinkage strains. The displacements as the result of shrinkage strains in the exposed edges are greater for the viscoelastic material than for the elastic material. As discussed earlier, significant stress gradients along the diagonal of the elbow geometry may be observed in the case of the viscoelastic material [Figure 12(b)]. At the same locations, the stresses in the elastic material, though relatively higher in magnitude, show little variation [Figure 12(a)].

It needs to be noted here that the stresses at the end of the first cure cycle, estimated from these simulations, plotted in Figure 11(a,b) (as well as Figure 12) are almost an order of magnitude higher than the typically observed tensile strengths (~60–80 MPa[22]) of structural epoxy resins which are employed as matrices in structural fiber reinforced composites, and also significantly exceed the highest magnitudes of residual stresses (~100 MPa[17]) reported in a cure simulation study of thick continuous-fiber-reinforced epoxy-matrix composites There are several assumptions in the current simulations that can contribute to

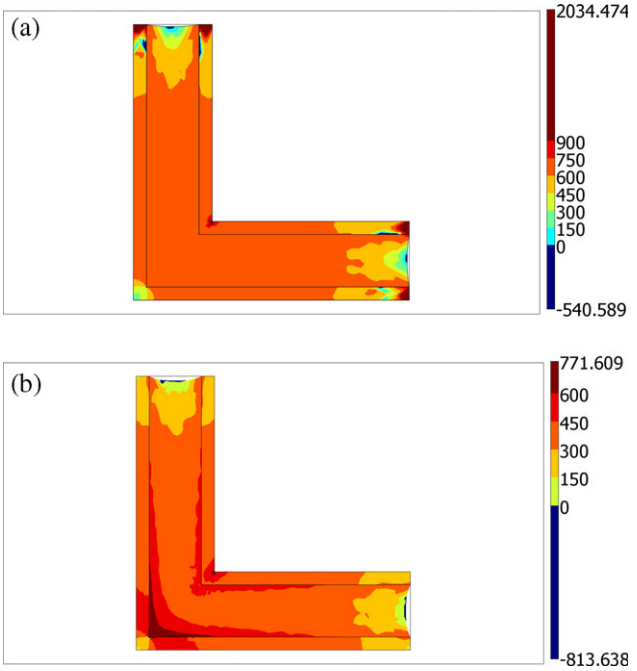

Figure 12. The contour map of the estimated maximum principal stress [MPa], and the deformation of the geometry, at the end of the first mold-constrained [cf. Figure 9(a,c)] cure cycle (at 10,000 s) estimated by employing (a) a linear elastic material model with a cure- and temperature-dependent resin elastic modulus, and (b) a viscoelastic material model with cure- and temperature-dependent resin relaxation spectrum. [Color figure can be viewed in the online issue, which is available at wileyonlinelibrary.com.]

these high estimates: (1) The thermal cycle that has been employed in these simulations covers temperatures which lie outside the experimental characterization temperature range (150–170°C) of Eom et al.[1] However, the same empirical relationships for temperature dependence of the modulus have been assumed to apply all the way to room temperatures. The room temperature elastic modulus at the limiting cure in this simulation, estimated using the extrapolation of the Eom et al. model, is 7.98 GPa. Considering that the Eom et al.[1] epoxy system is similar to the typical structural epoxies, the estimated modulus is about twice the typically reported room temperature modulus values for these epoxies.[22] (2) Moreover, the overall volumetric shrinkage (6%) and the coefficient of linear thermal expansion (100 ppm) have been set at the higher limit of the typically observed ranges for this material.[16,17] These assumptions would cause the overestimation of residual stresses by factors of 2–3. (3) Also, the current simulations are carried out only for the neat resin, and not a composite. In an actual continuous fiber-reinforced composite system, the matrix volume fractions are only 30–40%. The stresses associated with cure shrinkage, which occur only within the matrix, will be substantially reduced in the composite compared to the neat resin. The stresses due to thermal strains will also be reduced in the composite due to the lower coefficients of thermal expansion of the fibers which form the major component of the composite. Therefore, even though the results in Figures 11 and 12 suggest extensive damage in the epoxy resin, such stresses will not be achieved in composite systems of the same section thickness in which the epoxy matrix forms only a fraction. More importantly, these simulation trends also underscore the necessity to characterize the viscoelastic properties of the resin not only at cure temperatures but also at ambient and intermediate temperatures to avoid overestimation of residual stresses during cool-down.

The temperature, cure, and stress distributions, the latter shown in Figure 12, at the end of the first cure cycle provide the initial conditions for the second phase involving the heating of the cured elbow (after removal of the molds) under point constraints. The mechanical and thermal boundary conditions for this simulation are shown in Figure 9(b,d), respectively. The removal of the molds and the heating would result in the relaxation of the thermochemically induced residual stresses that developed under the constraint of the molds during the first phase of curing. Figure 13(a,b) shows the final shapes of the cured resin elbow at the end of the second heating cycle, predicted with cure-dependent elastic and viscoelastic models, respectively. Upon removal of the mold constraints, shrinkage of the arms of the elbow is observed with both elastic and viscoelastic material models. In case of the elastic material model [Figure 13(a)] the deformed concave shape of the short edges of the elbow instantaneously straightens out, indicating the release of elastic stored energy upon release of constraints. Moreover, for the elastic material model, in the absence of significant variation in stresses along the diagonal of the elbow (at the end of the first cure cycle), the residual stresses are relieved uniformly across the thickness of the elbow upon removal of constraints; this results in uniform shrinkage across the thickness of the part, and thus there is no shape distortion (or bending). As seen in Figure 13(b), in case of the viscoelastic material model, the deformed concave shape of the short edges of the elbow is maintained even upon removal of mold constraints and heating, indicating the relatively insignificant magnitudes of elastic stored energy due to viscoelastic relaxation of stresses. Moreover, for the viscoelastic material model, in the presence of large gradients in stresses across the diagonal of the elbow (at the end of the first cure cycle), the removal of mold constraints results in non-uniform shrinkage across the thickness of the part (with the maximum shrinkage occurring in areas corresponding to the maximum residual stresses), and thus there is significant shape distortion (or bending) in the viscoelastic material.

It is clear from the foregoing, that while the viscoelastic model leads to relatively lower stress estimates within the thermoset resin, it has more significant consequences in terms of capturing details associated with the evolution of severe stress-gradients during constrained cure of thick sections and the subsequent shape-distortion effects accompanying springback.

SUMMARY

The numerical implementation of the multiphysics problem, involving chemo-thermo-visco-elastic couplings, has been successfully demonstrated in the context of development and

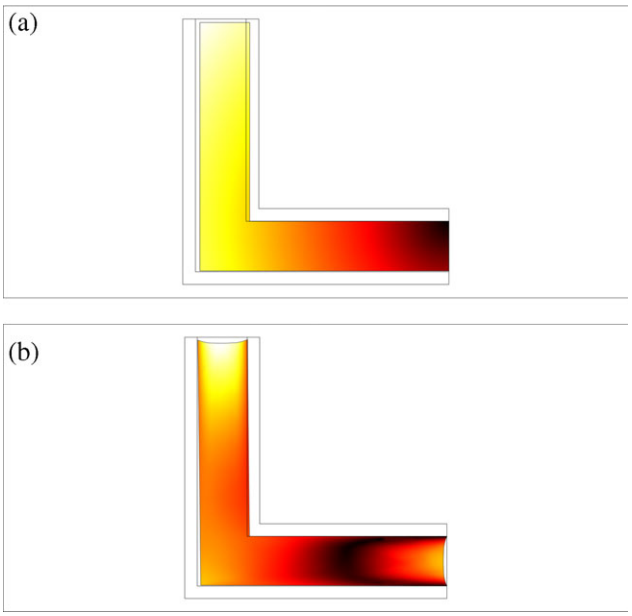

Figure 13. The surface map of total displacement, and the boundary deformation of the cured elbow geometry at the end of the second partially constrained [cf. Figure 9(b,d)] cure cycle (at 15,000 s) estimated by employing (a) a linear elastic material model with a cure- and temperature-dependent resin elastic modulus, and (b) a viscoelastic material model with cure- and temperature-dependent resin relaxation spectrum. [Color figure can be viewed in the online issue, which is available at wileyonlinelibrary.com.]

relaxation of mechanical or crosslink-shrinkage induced stresses in a curing epoxy-amine thermoset. Phenomenological aspects such as diffusion limited cure kinetics, incomplete cure, the viscoelastic behavior of the resin before as well as after the onset of gelation, and the evolution of the resin relaxation spectrum with the degree of cure have been captured in detail. The simulated trends in viscoelastic stresses at different degrees of cure and temperatures are compared and contrasted with those obtained from two additional equivalent material models—one involving a constant (cure- and temperature-independent) elastic modulus, and another involving a cure—dependent (but time-invariant) elastic modulus.

It is observed from these simulations that while the instantaneous stresses in a linear elastic material with constant or cure-dependent modulus, are only governed by the instantaneous states of temperature and degree of cure, the stresses in a viscoelastic material are strongly governed by the thermal history experienced by the resin. At equivalent final states of conversion and temperatures, it is seen that a viscoelastic resin typically develops lower degrees of stress as compared to an equivalent elastic resin, and also displays additional long-time relaxation even after achievement of the limiting conversions. More significantly, simulations with viscoelastic material model of residual stress development during cure of thick thermoset resin parts indicate that the spatial gradients in temperature and cure (enhanced by the exothermic heat of reaction) can result in significant spatial variation of viscoelastic residual stresses even after equilibration of the temperature fields and achievement of uniform cure; these subtle effects, which have a significant impact on the springback behavior, are not captured by simulations with elastic material models. These trends underscore the need for detailed and accurate viscoelastic material models for thermoset resins, adhesives, and composites for realistic estimates of residual stresses and springback behavior.

APPENDIX

COMSOL Multiphysics® Version 3.5a Subroutine Details for Implementation of the Model[11]

This section briefly describes the field settings that were employed within the relevant subroutines of COMSOL Multiphysics® Version 3.5a to implement the various aspects of the model to carry out the simulation of cure-induced residual stresses and springback in the thick elbow section (refer to Figure 9). The simpler load case implementations discussed in the context of Figures 5–8 employed similar field settings.

Curing Stage Simulation

Implementation of the Kinetics Model. The chemical kinetics model [eqs. (3)–(8)] was implemented using the standard "COMSOL Multiphysics" (Version 3.5a) module. The "Diffusion (Transient Analysis)" model was chosen from the "Convection and Diffusion" Application Mode of this module. The diffusion model was solved only within the "Curing Resin" subdomain (refer to Figure 9) as a purely time-dependent (spatially invariant) problem by setting the "Diffusion Coefficient (Isotropic)" to zero within the "Subdomain Settings." The "Reaction Rate" term was set to a logical expression shown below to capture the conversion dependent reaction rate defined by the kinetic model.

```
if(Conv<Conv_gel,Rate_Low_Conv,Rate_High_Conv)
```

In the above expression, Conv_gel = 0.7, Rate_Low_Conv is defined in eq. (3), and Rate_High_Conv is defined in eq. (6) (also refer to Table I). The boundary conditions at all the "Curing Resin" subdomain boundaries were set to "Insulation/Symmetry" (no material diffusion across the boundaries).

Implementation of the Heat Transfer Model. The heat transfer model [eqs. (37) and (38)] was implemented using the standard "COMSOL Multiphysics" (Version 3.5a) module. The "Conduction (Transient Analysis)" model was chosen from the "Heat Transfer" Application Mode of this module. The conduction model was solved within both the "Curing Resin" as well as the "Mold" subdomain (refer to Figure 9) in the "Transient Analysis" mode. Within the "Curing Resin" "Subdomain Settings," the "Heat Source" term was set to account for the exothermic heat of reaction [eq. (38)], using a logical expression to account for different kinetic regimes. This established the two-way coupling between the Kinetics and Heat Transfer models.

```
if(Conv<Conv_gel,-rho_smpn*DH_Reaction*
Rate_Low_Conv,-rho_smpn*DH_Reaction*
Rate_High_Conv)
```

In the above expression, DH_Reaction is the heat of reaction (refer to Table III) The heat cycle shown in Figure 9(c) was imposed as

the "Temperature" "Boundary Setting" in the form of a logical expression on all the exposed boundaries [see Figure 9(a)].

Implementation of the Viscoelasticity (Structural Mechanics) Model. The structural mechanics problem [eqs. (30) and (31)] was implemented using the "Structural Mechanics" Module (Version 3.5a). The "Transient Analysis" model was chosen from the "Plain Strain" Application Mode.

The "Mold" subdomain was modeled as "Isotropic" structural steel, and the material parameters listed in Table IV were entered in the relevant fields of the "Material" tab of the "Subdomain Settings." The automatic calculation of the thermal expansion stresses was activated for the "Mold" subdomain by activating the relevant fields within the "Load" tab of "Subdomain Settings."

The "Curing Resin" subdomain was modeled using the "Viscoelastic" Material Model. The shear relaxation modulus was defined as shown in eq. (17). In the "Material" tab of the "Subdomain Settings," the long term shear modulus (0.01) was specified in the field corresponding to "Shear Modulus." The moduli and relaxation times for the 34-coefficient Prony series were each defined separately as a "Global Expression. Each individual expression accounted for the relevant cure and temperature shift corresponding to the conversion regime [refer to discussion around eqs. (10)–(15), and also Table II]. The corresponding expression "Name" was entered within the fields specifying the Prony series "Branch" on the "Materials" tab of the "Subdomain Settings." A "Global Expression" corresponding to eq. (19) was entered in the field "Bulk Modulus." The automatic calculation of thermal stresses was not activated within this subdomain. Instead, both thermal as well as cure shrinkage strains were accounted for as given in eq. (40) by modifying the expression for the "Application Mode Subdomain Variable" "*p*" within the "Variables" tab of the "Equation System" "Subdomain Settings" as shown below

```
-K_smpn*(evol_smpn-3*CTE_mat*(T-373)-
3*(((1-DV_Shrinkage)^(1/3))-1)*Conv)
```

All the three "Physics" definitions, including the "Plain Strain" were solved in the "Transient Analysis" mode. It should be noted that a separate "Viscoelastic Transient Initialization" step was not required for the solution in this scenario since no high-strain-rate/step-strain type load was imposed on the geometry; since the thermochemical strains evolved over a relatively long time, the analysis could be treated as a pure transient analysis. The simulation was carried out for 10,000 s using the "Direct (SPOOLES)" solver with the "BDF" Method of "Time Stepping."

For the curing stage simulation, refinement of mesh was carried out to the extent that convergence of simulation was obtained. Of the three physics, conductive heat transfer was most sensitive to the relative coarseness/fineness of the mesh; with a very coarse mesh, the heat transfer simulation failed to converge when the onset of exothermic temperature rise occurred. To overcome this issue, a graded triangular mesh was employed, with relatively coarse meshing in the exposed edges of the elbow, and progressive refinement in the regions where the most significant thermal and stress gradients were expected (the elbow corners). The final mesh employed for the simulations was composed of 396 triangular elements.

Post-Cure Reheating-Induced Springback Simulation. After the mold-cure simulation described above, for the reheating phase, the thermal cycle shown in Figure 9(d) was imposed as the "Temperature" boundary condition within the "Conduction (Transient Analysis)" physics, on all the boundaries of the "Curing Resin" subdomain. Point constraints, as shown in Figure 9(b) were imposed using the "Point Settings" within the "Plain Strain (Transient Analysis)" physics. All the three physics were then solved using the "Restart" button within the "Solver" drop-down menu, this time only within the "Curing Resin" subdomain. The "Restart" option was used—combined with initialization of variables using the "Stored Solution" from the earlier cure phase—to enable accounting for the state of cure, temperature and stresses within the subdomain at the end of the mold-cure simulation. The solution was carried out in the time range 10,000–12,000 s using the "Direct (SPOOLES)" solver with the "BDF" Method of "Time Stepping."

ACKNOWLEDGMENTS

The author thanks Hamid Kia, Prakash Mangalgiri, and Sampath Vanimisetti for useful discussion. The author also acknowledges Prakash Mangalgiri, Pete Foss, and Arun Kumar for reviewing this article, and Sampath Vanimisetti for bringing several key references to his attention.

REFERENCES

1. Eom, Y.; Boogh, L.; Michaud, V.; Sunderland, P.; Manson, J.-A. *Polym. Eng. Sci.* **2000**, *40*, 1281.
2. Adolf, D.; Martin, J. E. *Macromolecules* **1990**, *29*, 3700.
3. Ferry, J. D. Viscoelastic Properties of Polymers; Wiley: New York, **1980**.
4. Gibson, R. F. Principles of Composite Material Mechanics; McGraw-Hill: Singapore, **1994**, p 285.
5. Williams, M. L.; Landell, R. F.; Ferry, J. D. *J. Am. Chem. Soc.* **1955**, *77*, 3701.
6. DiBenedetto, A. T. *J. Polym. Sci. Part B: Polym. Phys.* **1987**, *25*, 1949.
7. Hale, A.; Macosko, C. W.; Bair, H. E. *Macromolecules* **1991**, *24*, 2610.
8. Simon, S. L.; McKenna, G. B.; Sindt, O. *J. Appl. Polym. Sci.* **2000**, *76*, 495.
9. Prasatya, P.; McKenna, G. B.; Simon, S. L. *J. Compos. Mater.* **2001**, *35*, 826.
10. Hojjati, M.; Johnston, A.; Hoa, S. V.; Denault, J. *J. Appl. Polym. Sci.* **2003**, *91*, 2548.
11. *COMSOL Multiphysics Structural Mechanics Module Model Library*, Version 3.4; COMSOL AB: Stockholm, Sweden, **2007**, p 443.
12. Kamal, R. *Polym. Eng. Sci.* **1974**, *14*, 23.
13. Ryan, M. E. *Polym. Eng. Sci.* **1984**, *24*, 698.

14. Chern, C.-S.; Poehlein, G. W. *Polym. Eng. Sci.* **1987**, *27*, 788.
15. Timoshenko, S. P.; Goodier, J. N. Theory of Elasticity, 3rd ed.; McGraw Hills International Edition: Singapore, **1970**.
16. Zhao, L. G.; Warrior, N. A.; Long, A. C. *Mater. Sci. Eng. A* **2007**, *452–453*, 483.
17. Bogetti, T. A.; Gillespie J. W., Jr. *J. Compos. Mater.* **1992**, *26*, 626.
18. Adolf, D.; Chambers, R. *Polymer* **1997**, *38*, 5481.
19. Palmese, G. R.; Andersen, O. A.; Karbhari, V. M. *Composites A* **1999**, *30*, 11.
20. Michaud, D. J.; Beris, A. N.; Dhurjati, P. S. *J. Compos. Mater.* **1998**, *32*, 1273.
21. COMSOL Multiphysics Modeling Guide, Version 3.4; COMSOL AB: Stockholm, Sweden, **2007**.
22. DeTeresa, S. J.; Allison, L. M.; Cunningham, B. J.; Freeman, D. C.; Saculla, M. D.; Sanchez, R. J.; Winchester, S. W. *Report No. UCRL-ID-143287*, Lawrence Livermore National Laboratory, **2001**.